Solid particle erosion protection for the BLOODHOUND SSC front wheel arches

Chris J Hannon[1,2] and Ben J Evans[1]

Abstract

BLOODHOUND SSC is a World Land Speed Record Vehicle designed to travel at speeds of up to 1,050 mph (469 $m \cdot s^{-1}$), with the lower chassis and suspension extremely close to the ground. The shockwave from the nose of the car is expected to fluidise the desert surface of the track in Hakskeen Pan, South Africa. Sacrificial materials must be added to the exterior of the car to limit erosive wear. An open loop gas blast erosion rig was used to test materials at velocities predicted by Computational Fluid Dynamics in the front wheel arches, an area highlighted by the BLOODHOUND SSC engineers as requiring extensive protection. Tests of potential erosion protection materials were performed at 15° and 90° Impact angle using alumina as a substitute for Hakskeen Pan soil. Testing resulted in the use of a 2 mm thick Kevlar 49 laminate and 1.2 mm thick titanium Ti 15V-3Cr-3Sn-3Al sheet for the wheel arch liner, with titanium Ti 6Al-4V used for the wheel arch lip. The erodent mass flow rate for the application was an unknown variable during testing; the test rig used a specific erodent mass flow rate of approximately 300 $kg \cdot m^{-2} \cdot s^{-1}$. Depending on in-service erosion rates, the titanium liner may be replaced with either a more durable liner made from Stellite 6B or a less dense liner made from aluminium Al 6082-T6.

Keywords

Solid particle erosion, material characterisation, material selection, BLOODHOUND SSC, alumina

Chris J Hannon

(College of Engineering,) Swansea University, UK; SCA Industries Ltd, UK

Ben J Evans

(College of Engineering,) Swansea University, UK

Corresponding author

Chris Hannon, College of Engineering, Swansea University, Singleton Park, Swansea, SA2 8PP, UK
E-mail: christopherhannon1@gmail.com

1 Introduction

BLOODHOUND SSC is a World Land Speed Record Vehicle designed to travel at speeds of up to 1,050 mph (469 $m \cdot s^{-1}$), with the lower chassis and suspension extremely close to the ground. As the shockwave from the nose of the car shall fluidise the mud surface of the track, solid particles entrained in the high speed flow around the car shall have an erosive effect on the outer materials of the chassis and rear suspension. Testing of erosion protection materials in a representative environment was required to ensure that only suitable materials are used on the car.

The area of interest for the BLOODHOUND SSC engineers was the front wheel arches (Figure 1), as multiple electrical and hydraulic systems used to control the car are housed close to the arches. Ingress of soil in this region would lead to an unwanted weight gain and a high maintenance bill. The wheel arch conceptual design comprised a carbon fibre structural laminate and a 2 mm thick erosion resistant laminate co-cured with the

carbon fibre. In addition to this a removable metallic liner with a thickness of 1.2 mm would be used to protect the composite. A separate component was used on the lip of the wheel arches (Figure 1), which served the purpose of sealing any gap between the liner and the lower chassis. To maximise erosion resistance, this small component could be made from a material best able to cope with local flow conditions.

Computational Fluid Dynamics (CFD) analysis (1) suggested peak particle velocities would be below 200 $m \cdot s^{-1}$, which is within the capability of many gas blast and whirling arm erosion rigs used in helicopter rotor blade and oil and gas pipeline protection testing (2-5). Impact angles investigated were 15° and 90°. The literature indicated ductile erosion below 15° would be less than at 15° (2), and CFD analysis indicated Impact angles between 15° and 90° were unlikely to be encountered. An Impact angle of 90° was investigated as CFD analysis indicated this would exist at the Wheel arch lip. This paper details: the rig design; erodent selection; erosion rates by mass and volume for a variety of materials; and the downselection logic to select materials for the specific application.

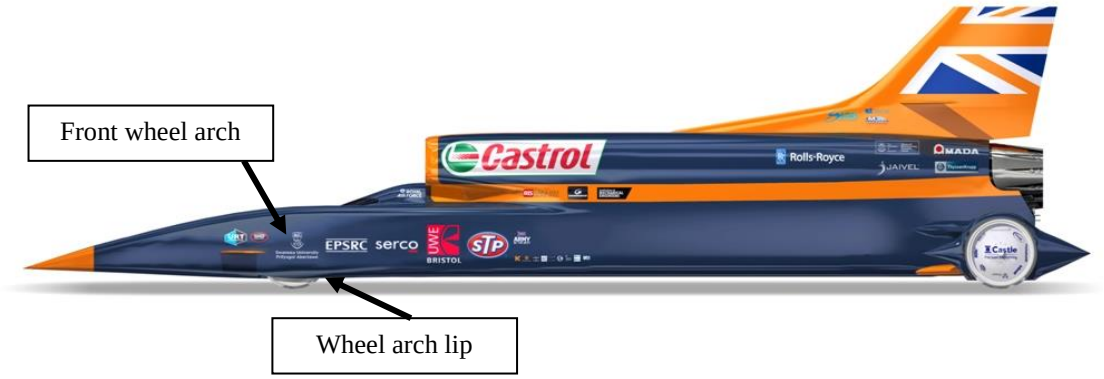

Figure 1: Side view of the front half of BLOODHOUND SSC, with the front wheel arches highlighted

2 Erodent selection

Only a relatively small (145 g) sample of Hakskeen Pan soil was available, meaning it was necessary to carry out erosive wear testing using a surrogate erodent. Figure 4 was generated using a Keyence Digital microscope (6) and shows that there is substantial variation in particle size for Hakskeen Pan soil. Particles with sizes above 1 mm were discounted from consideration as these were unlikely to become entrained in the flow. Characterisation of the soil was performed using a sieve shaker, accelerated for 15 minutes at approximately 10 g (98.1 $m \cdot s^{-2}$), with the following sieve apertures: 1 mm, 630 µm, 400 µm, 200 µm, 100 µm and 63 µm (7). The resulting mass of particles in each section of the sieve shaker was determined using an Adam PW214 analytical balance with ±0.3 mg accuracy and the results are plotted in Figure 2. The cumulative total exceeds 100 % due to retained particles in the apertures dislodging during testing, in spite of a rigorous brushing and washing procedure prior to testing. Approximately 80 % of particles had diameters less than 630 µm. In addition to the soil, small pieces of shale rock are also present in the desert. Both the Hakskeen Pan soil and shale have a Mohs hardness of approximately 7 (8).

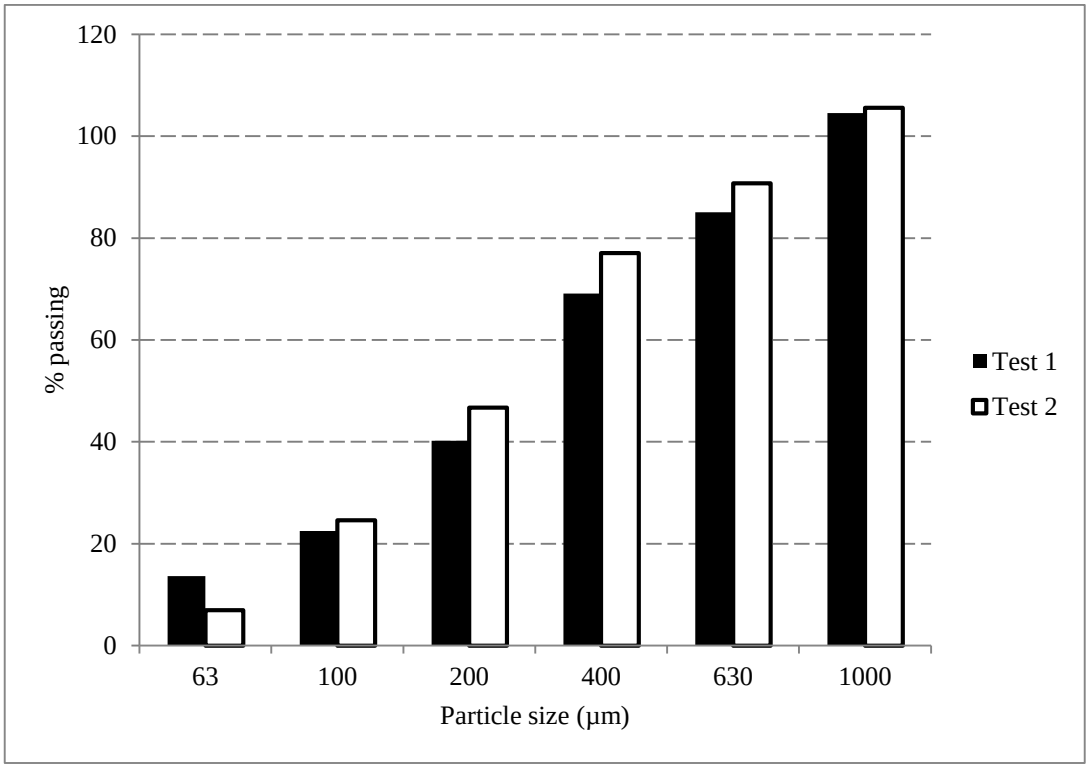

Figure 2: Cumulative undersize particle distribution of Hakskeen Pan soil sample

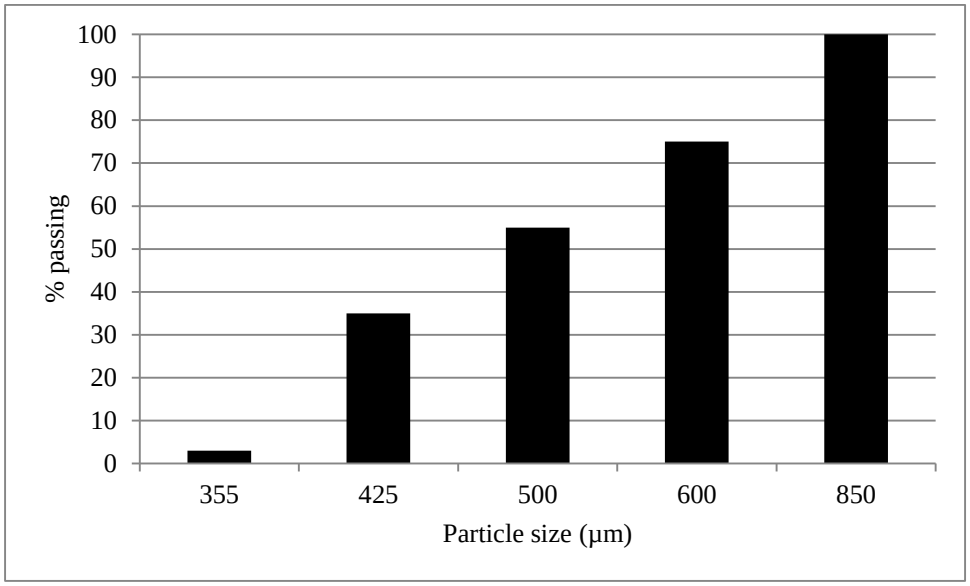

Figure 3: Cumulative undersize particle distribution of FEPA 36 abrasive (9)

White alumina was decided as a suitable surrogate erodent, due to its conservative Mohs hardness of 9 and its friable property mimicking that of the soil. A conservatively hard erodent was used to, in part, mitigate the risk of unknowns in the testing, such as the actual erodent speed. Average erodent particle size was agreed with the BLOODHOUND SSC engineers as 525 µm (Federation of European Producers of Abrasive Products (FEPA) 36) (10). The size distribution of FEPA 36 is shown in Figure 3, which matches the Hakskeen Pan distribution reasonably well. Larger particles would either not be entrained in the flow, or would most likely not be accelerated to velocities to be of concern, as erosion rate by elasto-plastic fracture is approximately proportional to particle velocity cubed (2). Figure 5 shows a sample of white alumina FEPA 36 and Hakskeen Pan soil sieved to between 400 µm to 630 µm. The particle sizes are a close match and the angularity of the alumina is higher, meaning that cutting action due to erosion by plastic deformation is likely to be conservative.

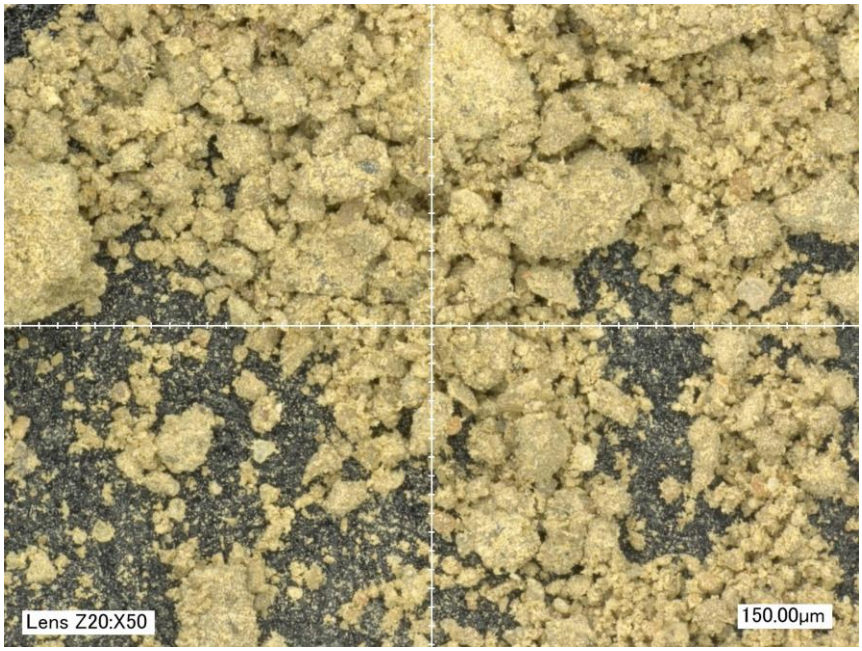

Figure 4: Hakskeen Pan soil sample showing the large range of particle sizes present

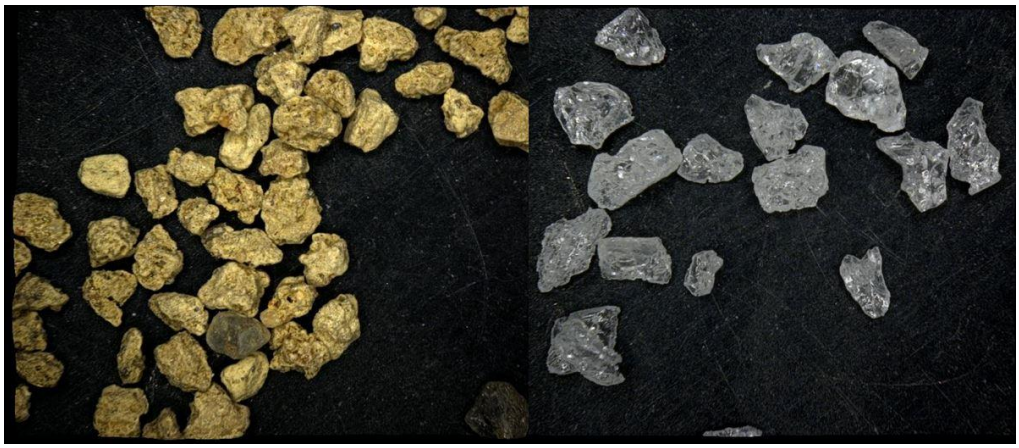

Figure 5: Hakskeen Pan soil, 400 µm to 630 µm sample (Left) compared with the white alumina erodent (Right), sieved to FEPA 36, used during testing.

3 Testing methodology

Several common approaches exist regarding solid particle erosion testing. Whirling arm erosion rigs affix samples to a blade tip, then spin the sample through a cloud of erodent (11). This method was not used due to higher equipment costs and safety implications. ASTM G76-13 provides the general architecture for gas blast erosion rigs, which is shown in Figure 6 (12). Due to key differences in the test conditions, such as internal nozzle diameter and particle velocity, this standard was used to inform testing decisions, rather than dictate them.

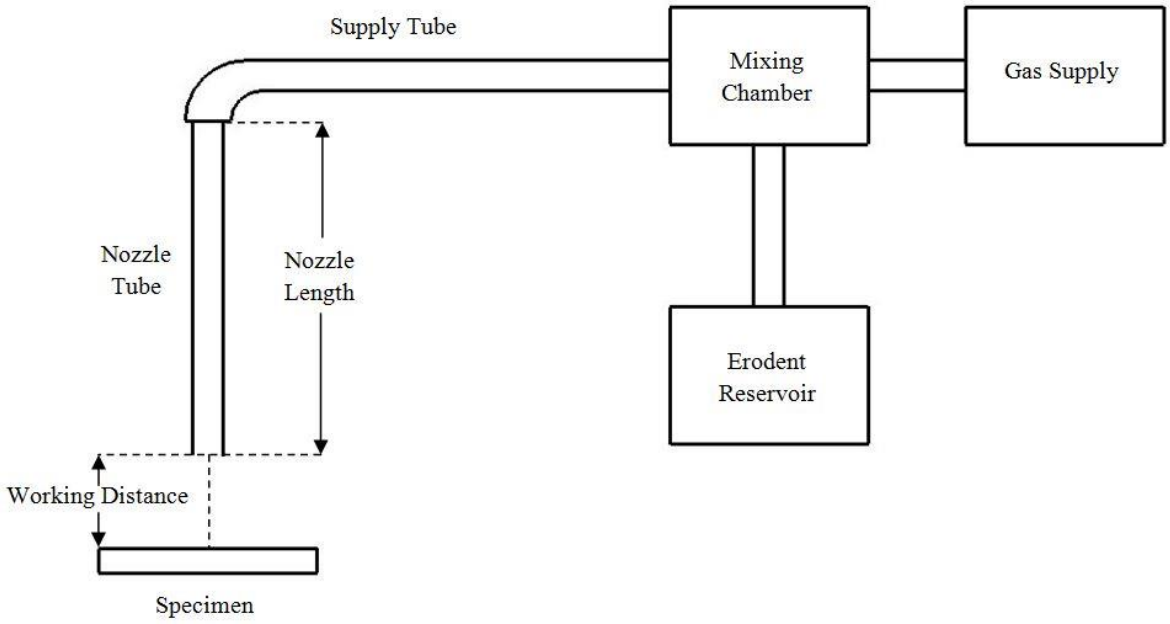

Figure 6: Generic gas blast erosion rig architecture, based on ASTM G76-13 (12)

The key unknown variable in the desert environment was the sand cloud density. The BLOODHOUND SSC operational environment is similar to that encountered by the main rotor blades of military helicopters, as rotor tips typically travel at Mach 0.6 in the hover. Taking off and landing in dusty conditions has demanded adoption of robust and cost effective materials (5, 13). However, the sand cloud density generated by helicopters was likely to be much less than that experienced by BLOODHOUND SSC, the floor of which is approximately 100 mm above the ground when stationary. For this reason metallic materials were instead recommended for consideration.

Whirling arm sand erosion rigs, typically used to test helicopter leading edge materials, have relatively low sand cloud densities of 0.5 $g \cdot m^{-3}$ (5). Based on sample geometry and test duration of 10 minutes this equates to an erodent mass per unit area of around 88 $kg \cdot m^{-2}$ and specific erodent flow rate of 0.147 $kg \cdot m^{-2} \cdot s^{-1}$. Gas blast erosion rigs for helicopter applications have used an erodent mass per unit area of up to 260 $kg \cdot m^{-2}$ with a specific erodent flow rate of 2.63 $kg \cdot m^{-2} \cdot s^{-1}$ (4).

A gas blast erosion rig, based on a commercially available open loop shot blaster with a 6 mm diameter, 35 mm long, ceramic nozzle and a working distance of 15 mm was used during testing. Flow conditions were provided via a compressed air cylinder with a multi-stage regulator set to 120 psig (827 kPa). The rig architecture was essentially identical to that recommended by ASTM G76-13 (Figure 6) (12). The rig was able to maintain specific erodent mass flow rates of approximately 300 $kg \cdot m^{-2} \cdot s^{-1}$, which for the typical test time of 30 seconds, equated to an erodent mass per unit area of 9000 $kg \cdot m^{-2}$. This was significantly higher than that used for helicopter erosion protection testing and was intended to address the uncertainty regarding the actual sand cloud density for the application. The test time of 30 seconds reflected the limited operational use of BLOODHOUND SSC, with run times over 950 mph expected to last approximately seven seconds.

Specific erodent mass flow rates above 100 $kg \cdot m^{-2} \cdot s^{-1}$ tend to lead to reduced erosion rates per particle, due to particles rebounding off a sample and hitting subsequent particles from the erosion rig nozzle (14). This was more of an issue for tests at 90° Impact angle (used for wheel arch lip testing), as the particles hitting coupons at 15° Impact angle rebounded away from the nozzle flux. The friable property of alumina meant rebounding particles were smaller and slower than those just exiting the nozzle, and so have less kinetic energy. This, combined with the change in erosion types at higher Impact angles, meant that testing at 90° Impact angle was still required (2).

Particles exiting the nozzle had an average speed of 132 $m \cdot s^{-1}$ (297 mph), with a standard deviation of 72 $m \cdot s^{-1}$ (161 mph). The relatively large standard deviation in particle velocity was due to the range in particle size. Particle velocity measurement was achieved via a 2 component Laser Doppler Velocimetry (LDV) system, which used a Stabilite 2017 ion laser with beam diameter of 1 mm, beam power of 0.5 Watts and wavelengths of 488 nm and 514.5 nm.

Samples used in the analysis were not subject to surface preparation techniques; rather, offcuts of material used in the construction of other parts of the car were tested wherever possible to ensure representative surface roughness was investigated. Painted samples were not tested as the wheel arches were not intended to be painted. Sample size was approximately 200 mm x 70 mm, with one sample typically being used for five tests at each Impact angle. The coupon was weighed using an Adam PW214 analytical balance with ±0.3 mg accuracy before and between tests to determine coupon mass loss. The region of the coupon immediately away from the focussed stream of particles from the nozzle was shielded using 3M 8671 Polyurethane Protective Tape bonded to the back of the coupon. Separation distance from the centreline of the nozzle to the coupon was approximately 15 mm for both test angles.

Table 1 details the composite materials tested at 15° Impact angle for the permanent wheel arch liner. The angle of particle flow was at 0° to the warp tow (90° to the weft tow) for all of the composite samples (15). Kevlar 49-1 had a 2x2 Twill weave and a fibre volume fraction of approximately 50 %. Kevlar 49-2 had a plain weave and a fibre volume fraction of 60 %, with the latter property intended to reduce the wear of the laminate due to the softer resin matrix. E glass fibres were in an eight harness satin weave and S glass fibres in a plain weave (15). These were chosen due to their low cost and, for the satin weave, superior drapeability (15). This was at the expense of high density and low fibre volume fraction. Carbon/Dyneema and carbon/Kevlar hybrids were also tested at the request of the BLOODHOUND SSC engineers. The resin used for all of the composite samples was MTC801 (16).

Table 2 details the metallic materials tested for the removable liner and also those considered for the aft wheel arch lip protection. SAE 4130 steel is widely used and was readily available to the BLOODHOUND Programme (17, 18). Stellite 6B is a cobalt base alloy used in applications requiring excellent wear resistance (19). Various titanium grades were tested, as these see application for leading edge erosion protection in aerospace applications (4, 5, 13). Aluminium Al 6082-T6 is not known for its erosion resistance; however, it was included in the study because of its low cost, low density and availability. DC01(1.0330) plain carbon “mild” steel was also tested as an additional low cost option. Nickel alloys and stainless steels were not considered due to lack of availability in the supply chain.

Surface roughness testing of uneroded samples was conducted using a Rugotest 1 roughness comparator, to BS 2634-2:2010, with accuracy of + 12 %, - 17 %. The Ra surface roughness for the metallic samples is included in

Table 2. The surface roughness of the composite samples was 0.2 µm in all instances.

As the erosion protection was intended to shield the systems inside the car and to reduce costly redesign effort, the geometry of the erosion protection would not be changed, only the material. This meant the metric of interest for this project was sample volume loss/mass of erodent ($mm^3 \cdot g^{-1}$).

Table 1: Composites characterised for wheel arch application (16)

Description	Resin content by weight (%)	Density of laminate ($kg \cdot m^{-3}$)
E glass (8HS M7781)	32	1895
Carbon Kevlar (Carbon T300/Kevlar hybrid 3 x 1)	43	1415
Carbon Fibre (T700 2 x 2 twill 12k)	40	1505
Kevlar 49-1	46	1325
Carbon Fibre/Dyneema (T300/Dyneema SK60)	50	1220
Kevlar 49-2	38	1352
S Glass	33	1835

Table 2: Metals characterised for removable liner and/or wheel arch lip

Description	Density ($kg \cdot m^{-3}$)	Surface roughness (µm)
SAE 4130 Normalised condition	7833 (17)	0.8
Stellite 6B	8387 (19)	0.8
Ti 15V-3Cr-3Sn-3Al	4761 (17)	0.8
Ti 3Al-2.5V	4480 (20)	0.8
Ti 6Al-4V	4429 (17)	0.4
Al 6082-T6	2700 (21)	0.4
DC01(1.0330) Steel	7861 (17)	0.4

4 Results and discussion

The following figures use error bars representing the maximum and minimum erosion rates encountered. The "X" in the middle of a result indicates the mean erosion rate, with the "box" of the "box and whisker" plot representing the three quartiles.

4.1 Composite erosion results – wheel arch laminate

As can be seen from Figure 7, the best composite material was the plain weave Kevlar 49-2, particularly on a volume loss basis. Its erosion mechanism at the 15° Impact angle was type I cutting, as can be seen in Figure 8 and compared favourably against the theoretical mechanism (2). Kevlar is a trade name for aramid fibres, which were designed to resist impact, which explains its superior performance during testing relative to other fibre types (22). The variation in the range of results for different composite materials is pronounced. The smallest range of results is for Kevlar 49-2, which also has the smallest resin volume fraction. E glass and S glass have a larger spread of results, despite the fibre volume fraction of just under 50 % being approximately equal to the other laminates (apart from Kevlar 49-2 and the carbon/Kevlar hybrid, which had approximately 60 % fibre volume fraction). The cause of the higher erosion rate for the E Glass fibre samples is most likely the eight harness satin weave, where eight warp tows ‘float’ over each weft tow, compared to a one-one ratio for a plain weave. This indicates that satin weave composites are particularly vulnerable to erosion and that the spread of results for the Glass fibre samples was due to a variation in where exactly the warp fibres were cut by the erodent particles.

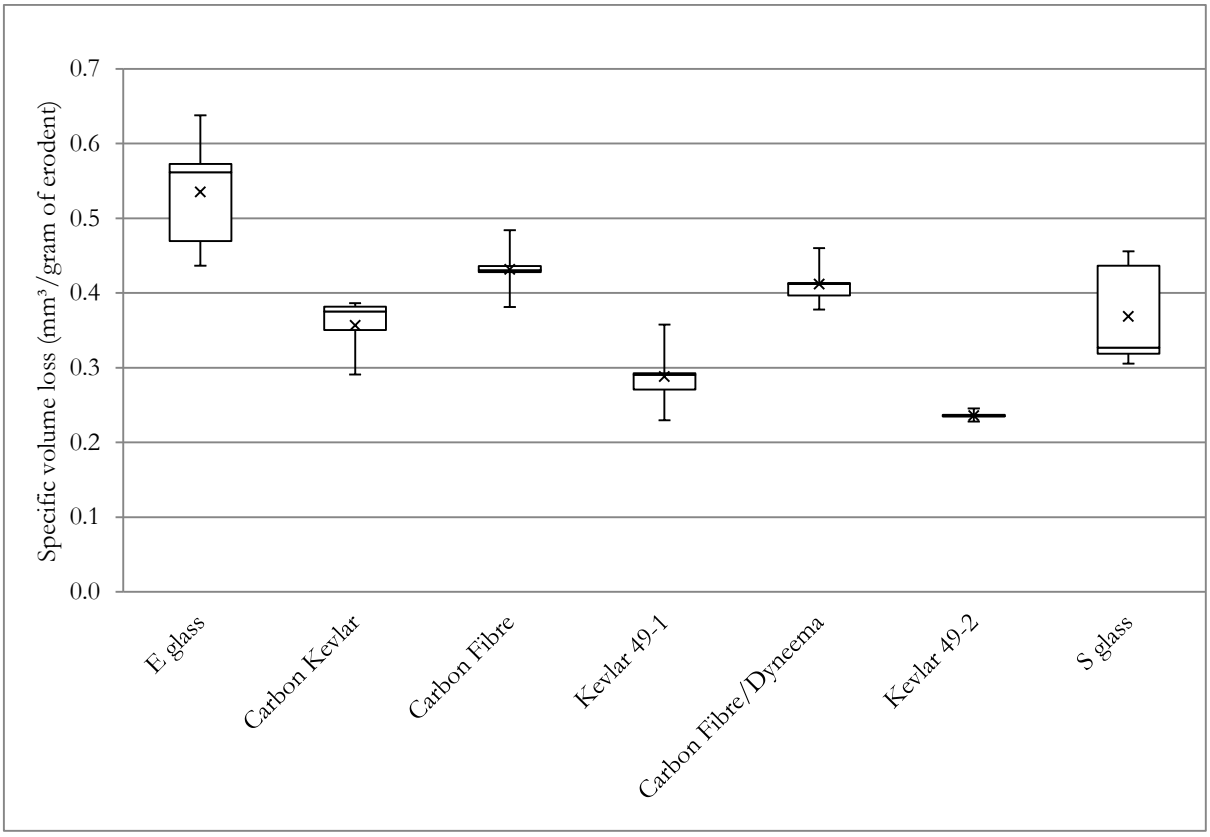

Figure 7: Composite volume loss erosion rates, 15° Impact angle, Alumina FEPA 36, 9000 kg·m^{-2}, 132 m·s^{-1}, error bars indicate range of results

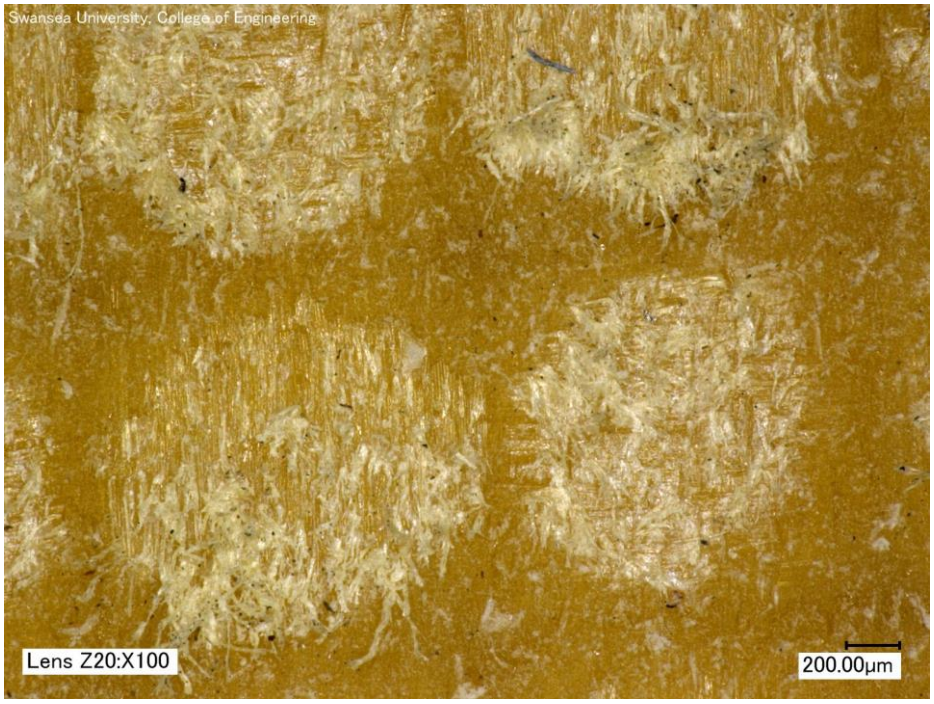

Figure 8: Kevlar 49-2 at 15° Impact angle, with type I cutting deformation evident.

4.1.1 Composite erosion impact crater scans

A Solutionix Rexcan CS+ system, using a 100 mm lens was used to scan the craters of the composite samples with a resolution of 0.012 mm. Scanning was not possible for the metallic samples as the impact craters were not of sufficient depth to allow resolution of the scan after application of Sprayable Chalk, used to reduce the reflectivity of the surface. A typical impact crater scan is shown in Figure 9. Table 3 summarizes the key dimensions of the impact craters for the different composite samples. The crater dimensions do not correlate well with the volume loss of the samples. For example, the craters for E glass were the shallowest; however, the profile of the crater was very smooth, indicating the satin weave of the sample allowed uniform removal of material. The twill and plain weaves of the other samples was less uniform, with pronounced ‘steps’ along

the length of the crater. This was likely due to the partially cut fibres collecting against a weft tow, with the loosely bundled fibres resisting further erosion. This effect was exaggerated due to erodent particles becoming trapped in the loose bundles, further enhancing erosion resistance and reducing mass loss of the sample. The majority of these particles were removed after testing by cleaning the sample with compressed air at 80 psig; however, some particles remained trapped within the sample.

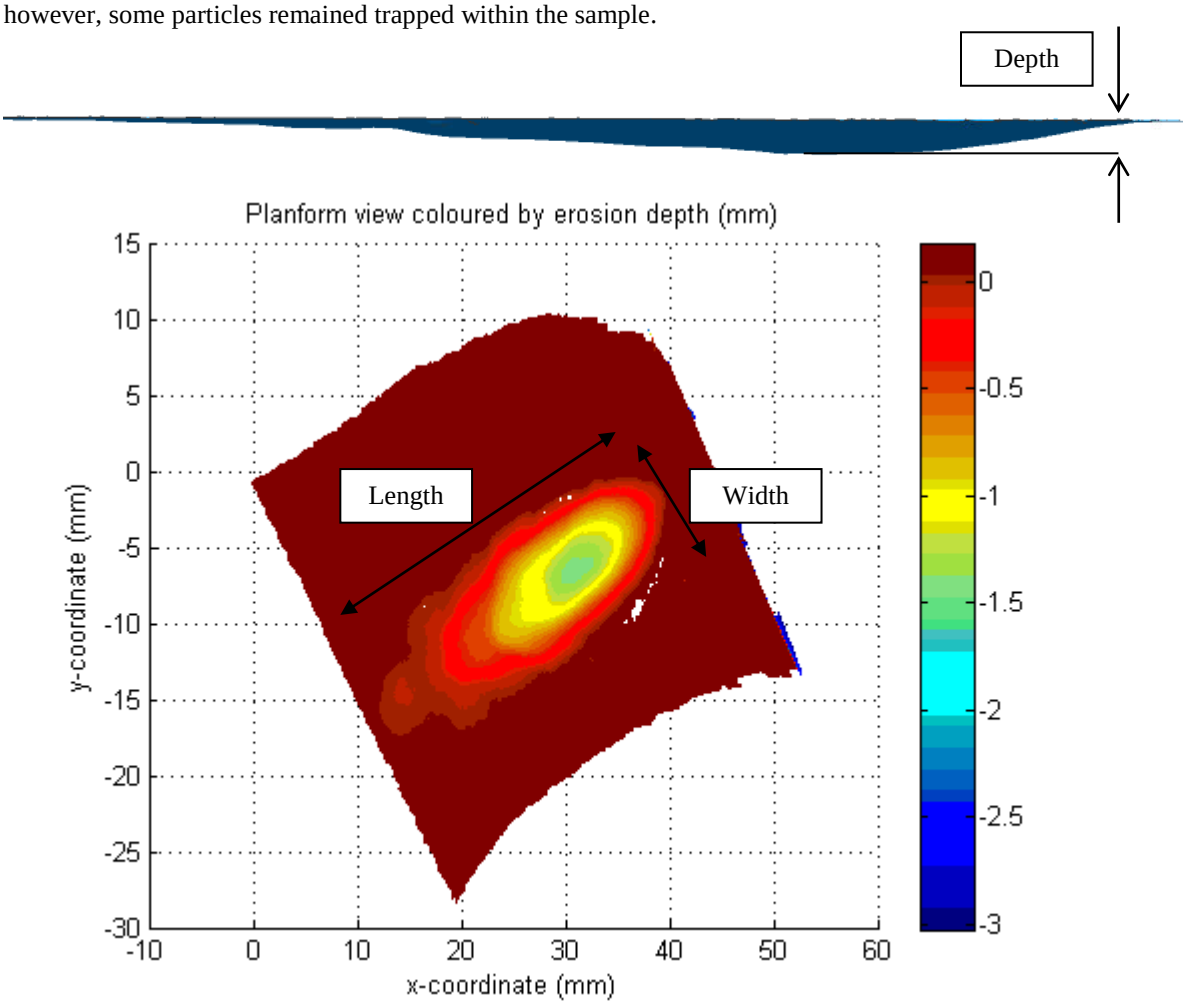

Figure 9: Digital scan of one of the Carbon Fibre impact craters

Table 3: Composite impact crater dimensions

Sample Name	Average maximum depth of crater (mm)	Width of crater (mm)	Length of crater (mm)
Carbon T300/Kevlar hybrid 3 x 1	1.05	9.9	19.9
Kevlar 49-1	1.21	9.6	23.0
Carbon T700 2 x 2 twill 12k	1.41	9.9	20.3
Carbon T300 Dyneema SK60	1.13	10.3	21.3
E glass 8HS M7781	0.94	10.4	22.0
S Glass Plain weave	1.52	10.3	24.5
Kevlar 49-2	0.97	8.7	21.4

4.2 Metal erosion results – removable liner

The metallic liner performance can be evaluated by Figure 10. Stellite 6B was superior on a volume loss basis, but was rejected due to its high cost and density. Figure 12 shows striations indicating Type II cutting of the Titanium 15V-3Cr-3Sn-3Al sample at 15° Impact angle. This was marginally the best titanium grade on a mass loss basis, which may be attributable to its metastable beta phase microstructure having a higher fracture toughness than the alpha-beta microstructures of the other titanium grades considered in this study (23). It also performed relatively better on a volume loss basis which was due to the higher vanadium content leading to an increase in density (Table 2). A similar explanation justifies the superior erosion performance of Ti 15V-3Cr-3Sn-3Al at 90° Impact angle (Figure 11), relative to the other titanium grades. Al 6082-T6 performed the worst of all the metals at 15° Impact angle, on a volume loss basis. This was due to its lower hardness, which made it susceptible to the cutting action dominant at this Impact angle (2).

Titanium 15V-3Cr-3Sn-3Al was chosen by the BLOODHOUND SSC engineers for the removable liner, due to its superior erosion performance and availability in sheet form in the BLOODHOUND SSC supply chain.

The composite facing plies were selected as Kevlar 49-2, again due to its superior performance. The limitation of this material is its poor repairability; however, its high resistance to erosion and flocculence when damaged makes it easier for inspections to identify a worn through metallic liner.

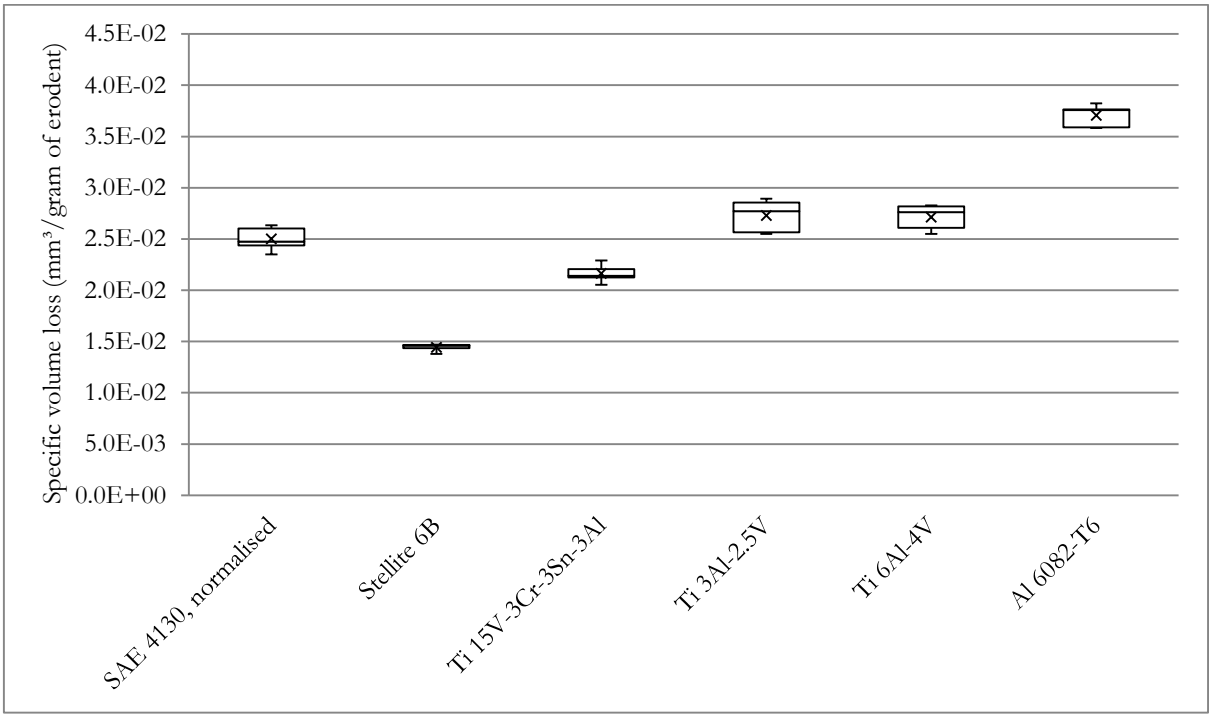

Figure 10: Metal volume loss erosion rates, 15° Impact angle, Alumina FEPA 36, 9000 kg·m-2, 132 $m \cdot s^{-1}$, error bars indicate range of results

4.3 Metal erosion results – wheel arch lip

Figure 11 show the erosion performance at 90° Impact angle, with Figure 13 showing a typical wear surface, which exhibited a roughened surface free of the cutting striations seen on samples eroded at 15° Impact angle. The roughened surface was essentially a series of overlapping impact craters, with material removal achieved

by brittle fracture. DC01(1.0330) steel had a mid-range erosion rate on a volume loss basis but was rejected due to a desire to reduce vehicle mass. Stellite 6B performed comparatively poorly at 90° Impact angle, which was attributed to its high Rockwell hardness of 33-43 HRC leaving it more susceptible to erosion by brittle fracture.

Al 6082-T6 eroded at approximately the same rate as Ti 15V-3Cr-3Sn-3Al on a volume loss basis, which was attributed to its high ductility. This ductility enabled it to sustain more particle impacts before the stress in sections of the sample surface exceeded the material tensile strength and local fracture occurred. This made it a potential candidate for the wheel arch lip protection, due to its lower cost and density. However, as the geometry of the wheel arch lip extended over a larger region than just the stagnation point, Ti 6Al-4V was chosen by the BLOODHOUND SSC engineers for this component. This grade was chosen over Ti 15V-3Cr-3Sn-3Al plate due to unacceptably long lead times, at the expense of an almost 50 % higher erosion rate on a volume loss basis.

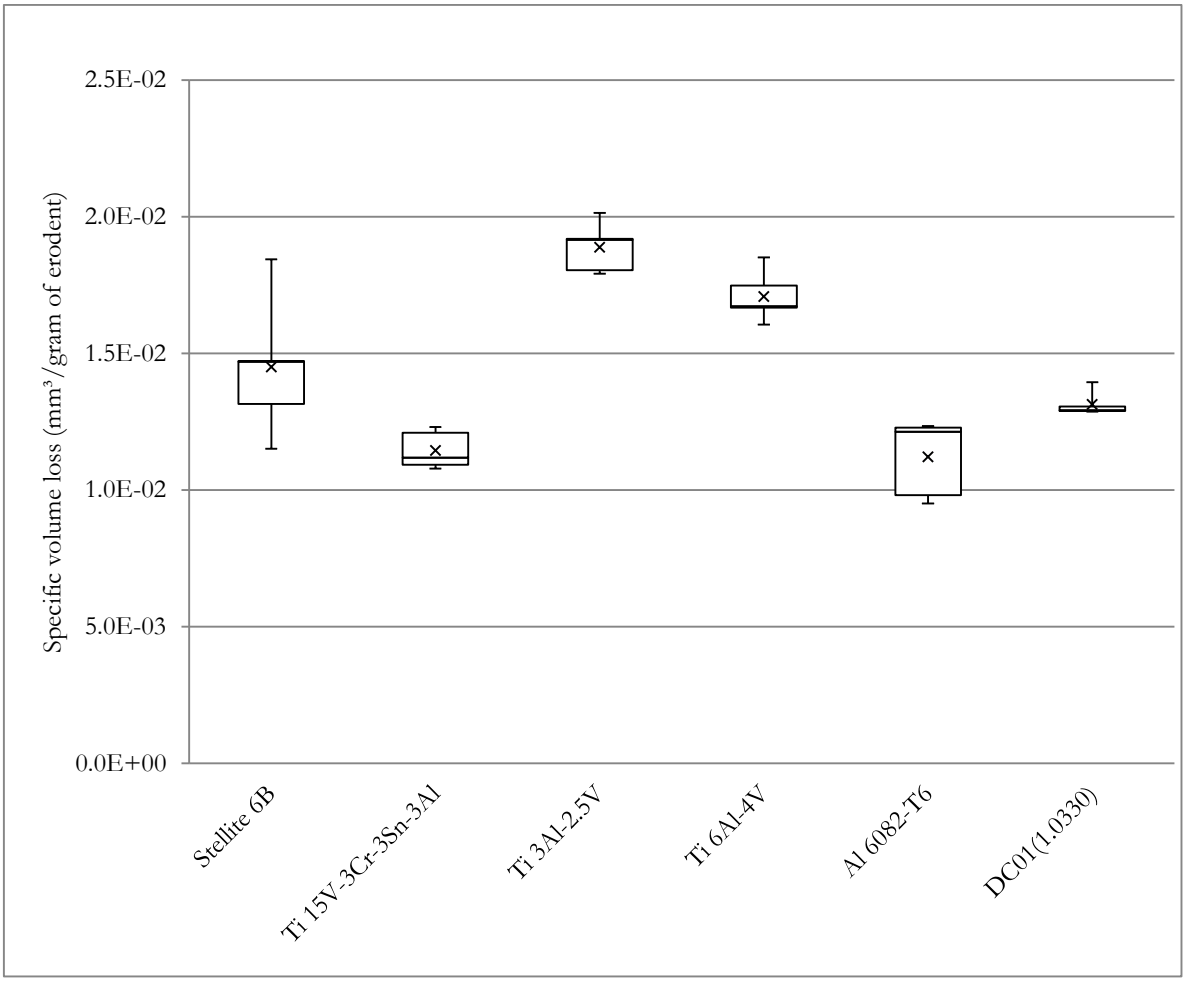

Figure 11: Metal volume loss erosion rates, 90° Impact angle, Alumina FEPA 36, 9000 kg·m-2, 132 m·s^{-1}, error bars indicate range of results

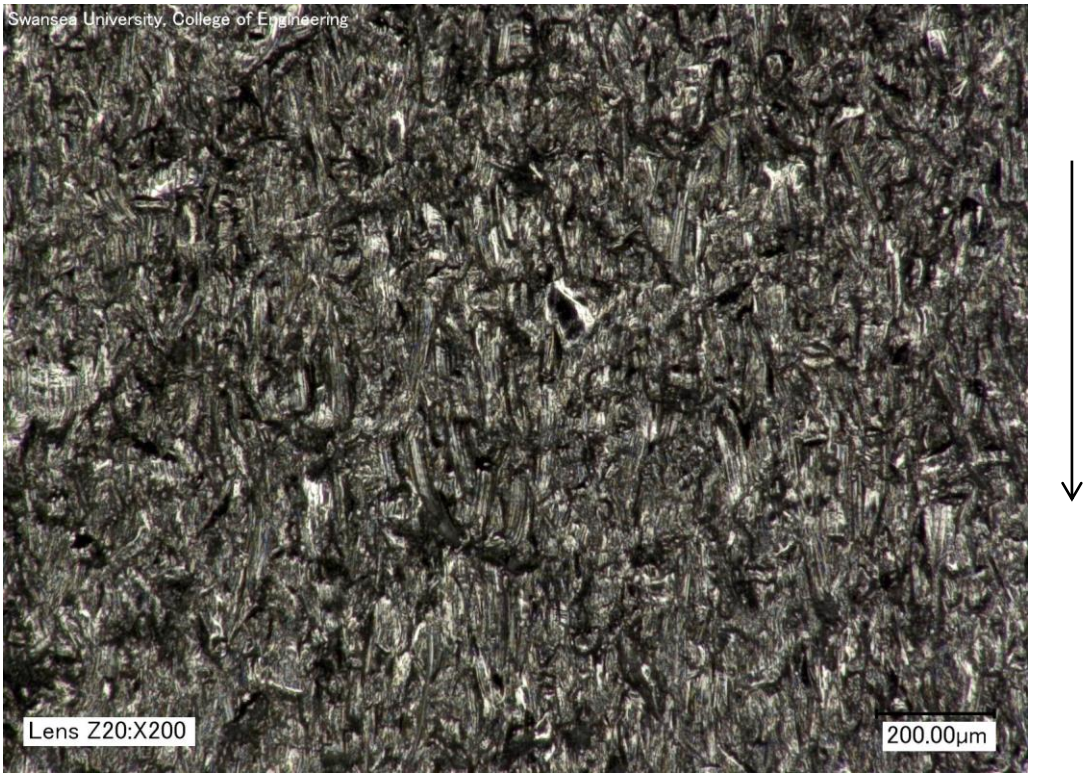

Figure 12: Ti 3Al 2.5V at 15° Impact angle, with cutting action evident. Particle flow direction is indicated by the arrow to the right of the figure.

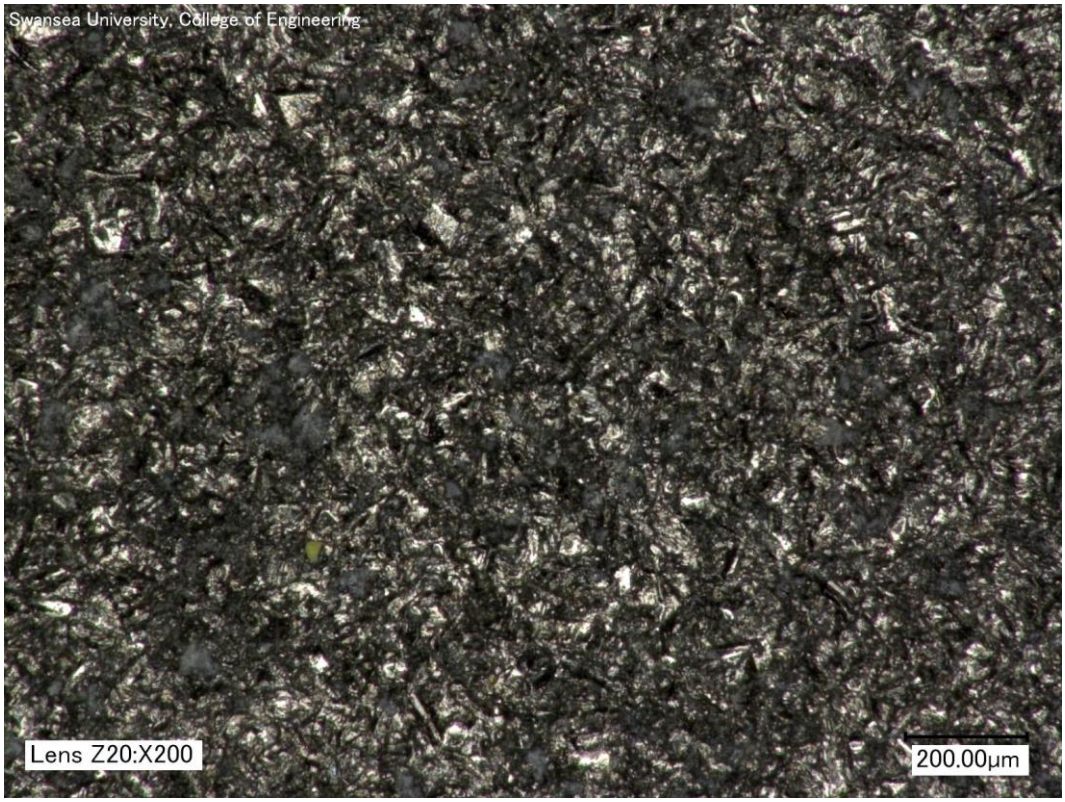

Figure 13: Ti 3Al 2.5V at 90° Impact angle, with impact craters evident.

5 Discussion

The erosion rate on the wheel arches shall be monitored by the BLOODHOUND SSC engineers and if erosion rates remain low once the vehicle has reached speeds above approximately 950 mph (425 $m \cdot s^{-1}$), then the removable liner and wheel arch lip may be replaced with one made from aluminium Al 6082-T6 to reduce vehicle mass. As the sacrificial liner comprises multiple components, a replacement liner could be fabricated out of different materials, with a less dense material used on the front half of the wheel arch. This concept was rejected for use on the initial liner, due to the need to validate the CFD model in the wheel arches, which may

differ significantly from reality due to simplifying assumptions. If erosion rate is higher than expected, then the BLOODHOUND SSC engineers shall either switch to using a Stellite 6B removable liner, or fabricate additional titanium liners for regular replacement.

The key outcome for this research project was the clear identification of erosion performance of a range of materials under conservative erosion conditions. This enabled selection of the most suitable metals and composite available for use on BLOODHOUND SSC, resulting in a more durable front wheel arch requiring less frequent inspections.

6 Conclusions

- Two materials, one a permanent composite laminate and the other a replaceable metallic liner, were required to protect the front wheel arches from solid particle erosion.
- A third material was used for the wheel arch lip, which was located at a stagnation point in the flow field, leading to impacts at 90° Impact angle, rather than the largely near tangential impacts expected within the wheel arch.
- Open loop gas blast erosion testing at conditions similar to CFD analysis of the wheel arches highlighted a plain weave Kevlar 49 laminate with a high fibre volume fraction as the best composite choice, and this was adopted by the BLOODHOUND SSC engineers. Stellite 6B sheet was the best material characterised for use on the removable liner; however, titanium Ti 15V-3Cr-3Sn-3Al was instead used to reduce cost and component mass.
- Plain weave composite samples typically had better erosion resistance, with a satin weave resulting in a significantly higher erosion rate.

- Titanium Ti 6Al-4V was used for the wheel arch lip, as this had good performance at 15° and 90° Impact angle, as well as relatively low density and ready availability.
- Aluminium Al 6082-T6 eroded at essentially the same rate as titanium Ti 15V-3Cr-3Sn-3Al at 90° Impact angle; however, its very high erosion rate at 15° Impact angle made it unsuitable for initial use on the wheel arch lip, as some of the flow would be at low Impact angle.

Acknowledgements

The authors would like to thank the national Centre of Advanced Tribological Studies (nCATS) in Southampton UK, for allowing us to inspect their erosion rig, and to the EPSRC Engineering Instrument Pool for use of the LDV system. Thanks to SHD Composites, Smiths Metals and Kennametal Stellite for coupon materials. Thanks are also due to Swagelok for sponsoring the pressure regulator for the rig. The support of the BLOODHOUND SSC engineering team was received with thanks.

Funding

The authors would like to acknowledge the funding from the EPSRC (EP/I015507/1) funded EDT MATTER - Manufacturing Advances Through Training Engineering Researchers, SCA Industries Ltd and the European Social Fund through the Welsh Government.

References

1. Evans BJ, Hassan O, Jones JW, Morgan K, Remaki L. Computational Fluid Dynamics Applied to the Aerodynamic Design of a Land-Based Supersonic Vehicle. Numerical Methods for Partial Differential Equations. 2011;27:141-59.

2. Hutchings IM. Tribology: Friction and Wear of Engineering Materials. UK: Edward Arnold; 1992.

3. Wood RJK, Wheeler DW. Design and performance of a high velocity air–sand jet impingement erosion facility. Wear. 1998;220(2):95-112.

4. Pepi M, Squillacioti R, Pfledderer L, Phelps A. Solid Particle Erosion Testing of Helicopter Rotor Blade Materials. Failure Analysis and Prevention. 2012;12(1):96-108.

5. Weigel WD. Advanced Rotor Blade Erosion Protection System. Bloomfield, CT: Kaman Aerospace Corporation, 1996 Contract No.: 19960924 006.

6. Keyence Digital Microscopes 2015 [[2015-04-07]. Available from: http://www.keyence.co.uk/products/microscope/digital-microscope/index.jsp.

7. British Standard. BS ISO 11277 Soil quality. Determination of particle size distribution in mineral soil material. Method by sieving and sedimentation. UK: BSI Group; 2009.

8. van der Waals J. Hakskeen Pan Challenge - 2 Soil Chemical Characteristics South Africa: Terra Soil Science; 2015 [2015-07-21]. Available from: http://www.terrasoil.co.za/education-bits.html.

9. ESK-SIC GmbH. E-Abrasic F4 to F220 Grain size distributions 2007 [2016-01-11]. Available from: http://www.esk-sic.com/uploads/images/schneid-schleif-und-poliermittel/E-ABRASIC-F4-bis-F220%20KV%20EN%2007_14_.pdf.

10. FEPA Abrasives. F grit sizes 2013 [2016-01-13]. Available from: http://www.fepa-abrasives.org/Abrasiveproducts/Grains/Fgritsizesbonded.aspx.

11. Department of Defense. MIL-STD-3033 Particle/Sand Erosion Testing of Rotor Blade Protective Materials. USA2010.

12. ASTM G76-13. Standard Test Method for Conducting Erosion Tests by Solid Particle Impingement Using Gas Jets. 2013.

13. Thomas WA, Yu C-J, Hong SC, Rosenzweig EL. Enhanced Erosion Protection For Rotor Blades. American Helicopter Society 65th Annual Forum; Grapevine, Texas, USA2009.

14. Arnold JC, Hutchings IM. Flux rate effects in the erosive wear of elastomers. Journal of Materials Science. 1989;24(3):833-9.

15. Baker A, Dutton S, Kelly D. Composite Materials For Aircraft Structures. 2nd ed. Schetz JA, editor. Reston, VA, USA: American Institute of Aeronautics and Astronautics, Inc.; 2004.

16. SHD Composite Materials Ltd. Wear Sample properties 2014 [2016-01-10]. Available from: http://shdcomposites.com/.

17. FAA. Metallic Materials Properties Development and Standardization. Battelle Memorial Institute; 2005.

18. American Society of Materials (ASM). ASM Metals Handbook Vol 4: Heat Treating. USA: ASM International; 1991.

19. Stellite K. Wrought Products Technical Data - Stellite 6B (AMS 5894) 2013 [[2015-05-14]. Available from: http://stellite.com/ProductsServices/Components/WroughtProducts/WroughtProductsTechnicalData/tabid/362/Default.aspx.

20. Smiths Metals. Titanium Grade 9: Ti-3Al-2.5V 2007 [[2015-05-14]. Available from: http://www.smithmetal.com/downloads/Ti9_SMC.pdf.

21. ThyssenKrupp Materials (UK) Ltd. Aluminium Alloy 6082 - Material Data Sheet 2013 [[2015-04-01]. Available from: http://www.thyssenkruppmaterials.co.uk/Downloads/Download_Files/Aluminium_Datasheets/6082.pdf.

22. DuPont. Kevlar 2010 [[2015-05-14]. Available from: http://www2.dupont.com/Products/en_RU/Kevlar_en.html.

23. Donachie MJ. Titanium : A Technical Guide. 2nd ed. Materials Park, OH, USA: A S M International; 2000.